International Journal of Neural Systems

INDIPENDENT COMPONENT DECOMPOSITION OF HUMAN MICRO-ECOG SOMATOSENSORY EVOKED POTENTIALS

IRENE REMBADO
Center for Translational Neurophysiology IIT@Unife, Istituto Italiano di Tecnologia, Via Fossato di Mortara 17-19, 44121 Ferrara, Italy
E-mail: Irene.rembado@iit.it
www.iit.it

ELISA CASTAGNOLA
Center for Translational Neurophysiology IIT@Unife, Istituto Italiano di Tecnologia, Via Fossato di Mortara 17-19, 44121 Ferrara, Italy
E-mail: Elisa.castagnola@iit.it
www.iit.it

LUCA TURELLA
University of Trento, Center for Mind/Brain Sciences (CIMeC), Via delle Regole, 101, 38123 Trento, Italy
E-mail: Luca.turella@gmail.com
http://www.unitn.it/cimec

TAMARA IUS
Struttura complessa di Neurochirurgia, Azienda Ospedaliero-Universitaria Santa Maria della Misericordia, Piazzale Santa Maria della Misericordia 15, 33100 Udine, Italy
E-mail: tamara.ius@gmail.com

RICCARDO BUDAI
Struttura complessa di Neurochirurgia, Azienda Ospedaliero-Universitaria Santa Maria della Misericordia, Piazzale Santa Maria della Misericordia 15, 33100 Udine, Italy
E-mail: budai.riccardo@aoud.sanita.fvg.it

ALBERTO ANSALDO
Graphene Labs, Istituto Italiano di Tecnologia, via Morego 30, 16163 Genova, Italy
E-mail: Alberto.ansaldo@iit.it
www.iit.it

GIAN NICOLA ANGOTZI
Neuroscience and Brain Technologies Department, Istituto Italiano di Tecnologia, Via Morego 30, 16163 Genova , Italy
E-mail: giannicola.angotzi@iit.it
www.iit.it

FRANCESCO DEBERTOLDI
Department of Neurosciences and Mental Health, Psychiatric Clinic, Fondazione IRCCS Ca' Granda Ospedale Maggiore Policlinico, University of Milan, Milan, Italy
E-mail: f.debertoldi@gmail.com

DAVIDE RICCI
Center for Translational Neurophysiology IIT@Unife, Istituto Italiano di Tecnologia, Via Fossato di Mortara 17-19, 44121 Ferrara, Italy
E-mail: davide.ricci@iit.it
www.iit.it

MIRAN SKRAP
Struttura complessa di Neurochirurgia, Azienda Ospedaliero-Universitaria Santa Maria della Misericordia, Piazzale Santa Maria della Misericordia 15, 33100 Udine, Italy

E-mail: miran.skrap@gmail.com

LUCIANO FADIGA
Center for Translational Neurophysiology IIT@Unife, Istituto Italiano di Tecnologia, Via Fossato di Mortara 17-19, 44121 Ferrara, Italy
Section of Human Physiology, University of Ferrara, Via Fossato di Mortara 17-19, 44121 Ferrara, Italy
E-mail: luciano.fadiga@iit.it
www.iit.it

High-density surface microelectrodes for electrocorticography (ECoG) have become more common in recent years for recording electrical signals from the cortex. With an acceptable invasiveness/signal fidelity trade-off and high spatial resolution, micro-ECoG is a promising tool to resolve fine task-related spatial-temporal dynamics. However, volume conduction – not a negligible phenomenon – is likely to frustrate efforts to obtain reliable and resolved signals from a sub-millimeter electrode array. To address this issue, we performed an independent component analysis (ICA) on micro-ECoG recordings of somatosensory-evoked potentials (SEPs) elicited by median nerve stimulation in three human subjects before brain surgery for tumor resection. Using well described cortical responses in SEPs, we were able to validate our results showing that the array could segregate different functional units possessing unique, highly localized spatial distributions. The representation of signals through the root-mean-square (rms) maps and the signal-to-noise-ratio (SNR) analysis emphasized the advantages of adopting a source analysis approach on micro-ECoG recordings, in order to obtain a clearer cortical activity picture. The implications are twofold: while on one side ICA may be used as a spatial-temporal filter extracting micro-signal components relevant to tasks for brain-computer interface (BCI) applications, it could also be adopted to accurately identify the sites of non-functional regions for clinical purposes.

Keywords: micro-ECoG, SEP, ICA, BCI

1. Introduction

Electroencephalographic recording from the surface of the cerebral cortex (electrocorticography, ECoG) has become a prominent tool in electrophysiology for both clinical and research purposes. ECoG recordings have been used to characterize neural activity subtending motor tasks [1], such as movements of a computer cursor over two dimensions [2], of individual fingers [3], of the whole arm [4], and even fine hand movements [5]. ECoG advantages over electroencephalogram (EEG) include larger signal amplitude and frequency bandwidth and higher stability [6], [7]. On the other hand, the need to obtain higher spatial resolution, comparable to what is obtained through penetrating electrodes, has driven technology to design high-resolution microelectrode arrays for ECoG recordings [8]. Furthermore, a high-resolution interface was made available by recently developed technology based on flexible silicon electronics [9], [10] allowing to concurrently define local cortical area specialization and large-scale cortical networks.

Although functional segregation is a well-established evidence of brain organization [11], [12], estimating neurophysiological current sources generating the electric fields recorded by micro-ECoG electrodes is still an unexplored path. In general, voltages recorded by surface electrodes - such as EEG and ECoG - may be modeled as a linear sum of independent current components [13], [14], [15]. An efficient technique is provided by Independent Component Analysis (ICA) [16] to decompose data into a set of maximally independent components linearly mixed to produce the original recorded signals. ICA was first applied by Makeig and colleagues [17] to decompose multi-channel EEG data, thus opening up new perspectives into complex event-related brain data. Other later studies have also pointed out ICA potential for isolating artifacts produced in EEG data by muscle activity and eye blinks [18], [19] and studying the dynamics of some pathological sources [20], [21], [22]. However, standard ECoG probes, typically used for clinical evaluation before epilepsy surgery [23], [24] and for accurate cortical mapping of ‘eloquent areas’ prior to tumor resection [25], [26], [27], [28], use electrodes with 1-10 mm^2 surface and 1 cm spacing. Consequently, even though abnormal component activity can be extracted by ICA decomposition, spatial resolution is often inaccurate.

In order to validate the ability of resolving features with higher spatial resolution using a new generation of microelectrode arrays, for the first time to our

knowledge, we used ICA to unmix independent sources of cortical data correlated to somatosensory evoked potentials (SEPs) collected across a spatial landmark - the central sulcus - by high density micro-ECoG recordings.

In particular, we developed an ad hoc 64 channels micro-ECoG array with electrodes having diameter of 140μm and an inter-electrode pitch of 600 μm. Data belong to three patients who underwent surgical procedures for tumor resection. Cortical SEPs, elicited by median nerve stimulation, are well known and widely used for clinical and research purposes [29], [30]. SEPs show a characteristic pattern for different recording areas: while in the motor cortex (M1) they show a positive peak at 18-23 ms (called P20) followed by a negative peak at 28-32 ms (called N30), in the somatosensory cortex (S1) the waveform is quite similar in timing but opposite in sign (i.e. N20 and P30, respectively) [31], [32]. This polarity inversion, called phase-reversal, is a functional marker of the central sulcus dividing M1 from S1 [32]. It is usually monitored during neurosurgical procedures to preserve somatosensory paths from surgical damage [30], [33], [34]. This well-known phase-reversal pattern at the level of the central sulcus was used as an anatomic-functional marker to spatially and temporally validate our results.

2. Materials and methods

Three patients with low-grade glioma located near somatosensory and/or motor cortical areas were enrolled for this investigation. The glioma size was measured from Navigator T1 of magnetic resonance images of the brain along the three axis were X= axial axis; Y=sagittal axis; Z=coronal axis.

Patient_1 was a 31-year-old male with left subcortical retrocentral low grade glioma (size of glioma for the 3 axes: X=8mm; Y=12mm; Z=11mm). The clinical diagnosis was made after the onset of complex partial motor seizures and secondary generalization.

Patient_2 was a 46-year-old male with recurrent left precentral low grade glioma diagnosed at routine clinical neuro-radiological follow-up (size of glioma for the 3 axes: X=26mm; Y=27mm; Z=31mm).

Patient_3 was a 61-year-old male with right parasagittal premotor low grade glioma (size for the 3 axes: X=43mm; Y=37mm: Z=46mm) diagnosed after a generalized seizure. The clinical data are summarized in Table 1.

Table 1. Clinical data

Patient	Sex	Age	Glioma location	Glioma size in mm	Diagnosis
1	M	31	Left subcortical retrocentral	X=8 Y=12 Z=11	Motor seizure
2	M	46	Left precentral	X=26 Y=27 Z=31	Routine clinical follow-up
3	M	61	Right parasagittal premotor	X=43 Y=37 Z=46	Generalized seizure

All patients gave their informed consent for cortical recordings and stimulation protocol. The protocol was approved by the ethical committee of Azienda Ospedaliera Universitaria Santa Maria della Misericordia (Udine, Italy) where tumor excisions were performed. Since the lesion was harbored in 'eloquent areas', the so called 'awake' surgery was performed (for technical details, see [26]) on all patients. This procedure, aimed to preserve essential cortical and subcortical eloquent structures while maximizing tumor resection [27], [28], was performed while the patient was conscious and aware of the surrounding environment. No patient showed motor or cognitive neurological deficits as assessed by neurological preoperative tests.

2.1 Microelectrode array and acquisition system

Recording microelectrode arrays were developed at the Italian Institute of Technology (IIT), specifically designed to provide higher spatial-resolution than the other standard clinical devices. Thanks to Flexible Printed Circuit Technology, the size of recording sites and inter-electrode spacing were reduced, while nanostructured gold coating would ensure low impedance [8], [35]. The 64 recording sites of 140 μm diameter were arranged in an 8x8 grid with 0.6 mm spacing for a total covered area of 4. 3 by 4.3 mm (see Figure 1-A, B). All signals were referenced to two inactive metal plaques placed on both sides of the recording area.

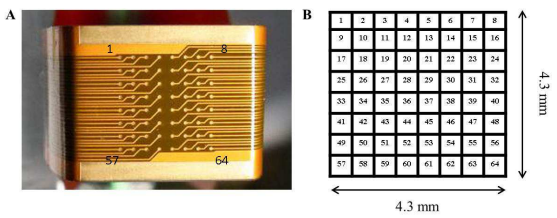

Fig. 1. Microelectrode array for ECoG recordings. A) Picture of microelectrode array for ECoG data acquisition. Each small dot corresponds to one electrode starting from electrode 1 (top-left corner) to electrode 64 (bottom-right corner) B) Schematic representation of relative positions of microelectrodes within the array when they are on the cortex surface, with recording area dimensions. The same electrode arrangement was maintained throughout the investigations reported in this paper.

Data were first amplified and then digitized at 3051.8 Hz, 24 bits of digital resolution, before being sent to an acquisition workstation for subsequent analysis. A total 22X gain was obtained with a two stage amplifier. The first stage, providing high input impedance and 11X gain, was integrated on a custom built head-stage directly connected to the microelectrode array. Amplified data were then wired to the second amplification stage featuring a band-pass filter (1Hz-1500Hz) with an additional 2X gain factor. Finally, Transistor-Transistor Logic (TTL) signal, provided by the stimulation system for time synchronization with external trigger, was digitized at the same sampling rate used for ECoG data.

2.2 Impedance Measurement

The impedance of the micro-ECoG contacts was systematically measured before surgery by galvanostatic electrochemical impedance spectroscopy (GEIS), performed in saline physiological solution (0.9% NaCl), by applying a current (sine wave) of 300 nA RMS at 10 frequencies per decade over the range 1-10^5 Hz. GEIS was carried out using a potentiostat/galvanostat (PARSTAT 2273, Princeton Applied Research) connected to a three-electrode electrochemical cell with a platinum counter electrode and a Ag/AgCl reference electrode.

2.3 Array location

In all patients, cortical recordings were carried out during awake surgery for low-grade glioma resection near somatosensory or motor areas. Neural signals were collected before beginning surgical procedure, and immediately after opening the dura. The placement of the recording array was based on information collected from different preoperative surveys. As part of standard surgical protocol, patients had undergone a series of fMRI scans in order to define functional brain networks. Those data were entered into the neuro-navigation system (Stealth Station, Medtronic, USA, http://www.medtronic.com/) in order to determine the site of these regions during surgery. In addition, cortical areas were mapped by the neurosurgeon through Direct Electrical Stimulation (DES), a methodology previously described by Ojemann and Berger [26]. With DES, a real-time functional map of the brain could be produced by applying electrical current directly on the cortex surface with a bipolar stimulator. Current intensity was adjusted to each patient and determined by progressively increasing the amplitude by 0.5mA steps, from a 1mA baseline until a sensory-motor response was elicited. Within the motor area, DES evokes movements of the contralateral side of the body, and, if applied on the somatosensory area, it evokes a sensory response (see Figure 2-A). Finally, during surgery, also continuous intraoperative neurophysiological monitoring of SEP responses was required. This was done by using standard cortical strips typically featuring eight electrodes with one centimeter of inter-electrode spacing. Since lesions were located near somatosensory and/or motor cortical areas, SEPs elicited by median nerve stimulation were continuously monitored by a clinical neurophysiologist. Cortical SEPs, obtained by averaging neural signals triggered by stimulation, are univocally described in terms of P20-N30 and N20-P30 patterns, depending on recording site. While the former ones are recorded from the motor cortex, the latter ones are recorded from the somatosensory cortex. Consequently passing from one area to the other, the evoked neural activity changes polarity, and this so-called ‘phase reversal’ is used as a functional marker of central sulcus during functional monitoring [29], [32], [33]. Thus, while DES provides an approximate identification of M1 and S1, ECoG signals recorded by these standard cortical strips allow to better identify the central sulcus path by means of the electrodes where the ‘phase reversal’ is observed.

Based on these pre-resection data, the microelectrode recording arrays have been correctly placed across the central sulcus (see Figure 2-A).

2.4 SEP stimulation protocol

Median nerve stimulation was triggered by a dedicated computer delivering a TTL signal to both the stimulator and the acquisition system. Nerve stimulation was conducted on the wrist contralateral to the cortical recording site. Stimulation parameters were set following the guidelines of the American Clinical Neurophysiology Society by using a train of single pulses at 3.3 Hz frequency rate, 10 mA mean current intensity and 200 µs duration [36]. Stimulation intensity was always set above the motor threshold, inducing a twitch of the thumb in all patients. Patients were instruct ted to remain still and relaxed throughout the entire stimulation session.

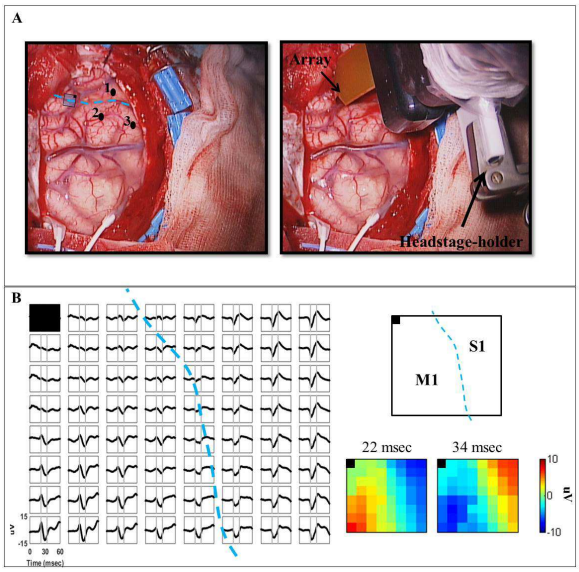

Fig. 2. Array location and SEP activity for Patient_1. A) Photographs of surgical microarray placement. Left: cerebral cortex before array placement with cortical points where DES had evoked a response; 1- index movement, 2- thumb tingling, 3- index tingling. The array, schematically represented by the small square, was placed on the central sulcus (dotted blue line). Right: array placement. The side of the headstage-holder provides array orientation on the cortex. B) Average SEP activity for each electrode (plotted data show the 60 ms of signal after the stimulation onset). Electrode arrangement reflects actual electrode position within the array and on the cortex (the black square in each array representation indicates the position of electrode 1). Two vertical lines in each plot point out the timestamp at 22 msec and 34 msec., respectively. The central sulcus path (dotted blue line) can be traced by following the progressive phase reversal among electrodes. Insets: color maps of recorded voltages for all electrodes at 22 msec and 34 msec. There is a clear difference in timing and polarity between lower left and upper right corners of the array which is used to validate the identification of cortical areas (i.e. M1 and S1).

2.5 Data pre-processing

Data analysis was performed using MATLAB built-in and custom-built functions (Mathworks, www.mathworks.com) and adopting freely available EEGLAB Toolbox [37], (http://sccn.ucsd.edu/eeglab/). ECoG data were pre-processed before subsequent analysis by removing any artifacts induced by median nerve stimulation, and adopting an interpolation method substituting a two millisecond artefact with the mean activity during the two milliseconds before and after it. Channels showing abnormal activity were excluded from further analysis based on visual inspection of recorded micro-ECoG data. Finally, each data set was re-referenced on the common average.
Data have been segmented into epochs of 160ms time-locked to the stimulation (ranging from 100ms before the onset to 60ms after it). To obtain homogeneous samples, 360 epochs of SEPs, corresponding to about two minutes of median nerve stimulation, were selected for each patient for further analysis. For Patient_1, only 250 epochs were selected due to his movements during acquisition. We didn't down-sample the data because high frequencies oscillations (HFO) are characteristic of SEP signals [39.

2.6 Independent Component Analysis (ICA)

In order to decompose channel data into the same number of independent signals, we used ICA algorithm based on an "infomax" neural network, firstly described by Bell and Sejnowski [16] and implemented for EEG data by Makeig and collaborators [17]. Considering X(t) the set of recorded time series, the algorithm returns an unmixing matrix W by minimizing the Mutual Information of random vectors resulting from a linear transformation of mixed signals X(t) and followed by nonlinearities. In this way, redundancy between output units can be minimized [16]. When W multiplies mixed signals X(t), it decomposes data into a matrix of

independent component (IC) time series, S(t), of the same size as the input data.

$$W*X(t)=S(t) \quad (1)$$

By multiplying IC activations with W-inverse (Eq. 1), the original data channel is back-projected or restored.

$$X(t)=W(-1)*S(t) \quad (2)$$

W-inverse is the component mixing matrix, whose columns provide the relative strengths and polarities of projections of one component source signal to each of the recorded channels (Eq. 2) [40].

2.7 Pairwise correlation

Correlation analysis based on coefficient of determination (R square) was computed between pairs of electrodes or pairs of components. For this investigation, the square value of Pearson's correlation coefficient (r) was adopted as coefficient of determination. Pearson's r is a statistical quantity measuring the strength and direction of a linear dependence between two X and Y variables.

In our case, X and Y are the recorded data and R square value is the strength of the relationship between the two signals without any polarity definition. It is a useful measure because, ranging from 0 to 1, it assesses the similarity between the two signals.

For correlation estimates the averages over all selected epochs of each non discarded electrode (i.e. SEP responses) and the component activations were considered. For each electrode pair and for each component pair, the R square was calculated and two distributions were conveyed and compared. Only significant values ($p<0.05$) were reported.

2.8 Percent variance accounted for (PVAF)

Extracted components contribute with different weight to channel signals, which we quantified in terms of 'percent variance accounted for' (PVAF). PVAF conveys the relationship between electrode and component, providing a numeric value of correlation strength with all channel signals for each component. Every recorded signal is totally reconstructed by back-projecting all independent component activations and consequently, despite different component contribution to channel data, their total sum provides a PVAF equal to 100% for every signal.

From a mathematical point of view, given component k and signal Xi(t) of electrode i, component k back-projection on channel i is defined as:

$$Xj,i(t)= Wj,i(-1)*Sj(t) \quad (3)$$

Where W(-1) is the ICA mixing matrix and Sj(t) is the activation time series of the jth component (Eq. 3).

This allows to calculate PVAF of component j to the signal of electrode i as:

$$PVAF(j,i) = \left[1 - \frac{var(Xi(\cdot)-Xj,i(\cdot))}{var(Xi(\cdot))}\right] * 100 \quad (4)$$

2.9 Root-mean-square (rms) maps and Signal-to-Noise Ratio (SNR) analysis

In order to establish whether ICA provides a substantial improvement in understanding a neural pattern already visible by averaging the signal over several trials, we calculated for each electrode the root-mean-square (rms) of SEP signals and the rms of the back-projection of the component which best fits the location of the central sulcus (we refer to this component as phase-reversal component). For both signals we generated a color map representing the rms values for all electrodes. To provide a quantification in term of signal-to-noise ratio (SNR) of such improvement, we compared SNR values for all electrodes. Consistent with previous works [41], [42], [43] we defined as signal (S) the peak-to-peak amplitude of the averaged signal in the range of [0-60] ms from the stimulation onset and as noise (N) the rms of 100 ms of signal before the stimulation onset. Thus we calculated for each electrode the SNR as: SNR = S/2*(N). To show the result we used a color map, plotting for each electrode the difference between the SNR of the phase-reversal component and the SNR of SEP.

3. Results

3.1 Phase reversal at sub-millimeter scale

SEPs for Patient_1, averaged over all trials, are shown in Figure 2B. The array provided a sub-millimeter spatial distribution of ECoG on the cerebral surface. Due to phase reversal, the central sulcus location and path could be identified with high precision in all patients, as represented by dotted blue lines. While the recording cortical site was anatomically similar for all patients, differences among patients in craniotomy, due to surgical approach, determined different orientations of recording arrays and consequently of sulcus trajectories on the arrays.

In particular for Patient_1, the border was located between the left and right side, of the matrix vertically dividing the array. More specifically, between electrodes 57 and 8 (diagonal direction on the array), a clear phase reversal from 22 ms to 34 ms could be observed (see Figure 2B).

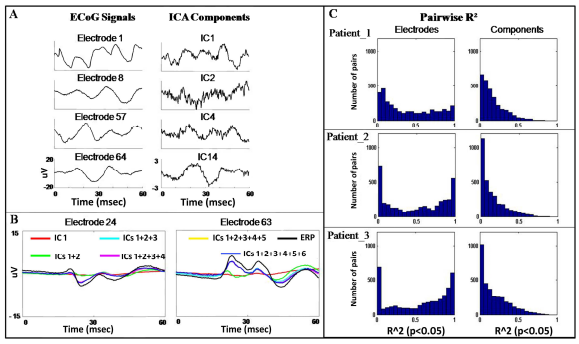

Fig. 3. Comparison between electrode signals and independent components. A) Single trial SEP (left) and ICA (right) for four representative electrodes of Patient_1. B) Contribution of four components progressively added to the signal of two representative electrodes for Patient_2. C) Histograms of pairwise R^2 between electrodes (on the left) and ICs (on the right) returned from ICA for all patients. The X axis represents the R^2 values ($p<0.05$) and the Y axis represents the number of pairs. The plots show that the distribution of the number of independent component pairs is shifted towards zero R^2 for all patients. This means that the similarity between time series waveforms is greatly reduced if we consider components instead of electrode signals.

3.2 Reduction in pairwise R2 of independent components when compared to electrode signals

After extraction of independent components from recorded data, we first asked whether ICs time series were statistically less correlated than the time series of the corresponding microelectrode signals (see Figure 3). To answer this question, we calculated pairwise R^2 between all pairs of average SEP channels and between all pairs of relative IC time series. Only significant values ($p<0.05$) were considered. In Figure 3-C, the results are shown with two histograms for each patient: the first related to the electrode pairs and the second related to the component pairs. From a statistical point of view, the analysis quantifies, in terms of mean and median distribution (see Table 2), a reduction in waveform similarity of independent components compared to original electrode signals.

Table 2. Statistics related to histograms of pairwise R2 for all three patients.

Patient	Type of pairs	N pairs ($p<0.05$)	Mean R^2	Median R^2	Range R^2
1	Electrodes	3422	0.4098	0.3314	Min: 0.0211 Max: 0.9998
	Components	2898	0.1710	0.1249	Min: 0.0211 Max: 0.8127
2	Electrodes	3825	0.4994	0.5447	Min: 0 Max: 0.9988
	Components	3193	0.1538	0.0995	Min: 0 Max: 0.8491
3	Electrodes	3897	0.5603	0.6568	Min: 0 Max: 0.9999
	Components	3357	0.1890	0.1356	Min: 0 Max: 0.8838

3.3 Relationship between electrodes and components and advantages of extracting ICs

The relationship between electrodes and components was quantified through the "percent variance accounted for" (PVAF). As previously described, with PVAF the contribution of independent components to the original signal of every electrode can be calculated. Figure 4 shows the percent variance accounted for some components to the signal of all electrodes for Patient_1. One color map was obtained for every component by outlining the electrodes in their relative positions within the geometry of the recording device. A green scale was adopted: electrodes shown in light-green have the highest PVAF. If recorded signals were totally independent, the components would be localized only on one electrode providing 100% variance. Instead, each component contributes to the signal of several electrodes defining its own characteristic spatial pattern. The back-projection of the components on all electrodes confirms this fact (see Figure 5). This means that signals from microelectrodes are not independent and that they do not arise from the activity of wholly separate cortical domains. Components are not randomly distributed in space and their distribution has a significant biological meaning. In figure 4 the color map of IC14, for example, seems to follow the central sulcus as confirmed by its back-projection activity on all electrodes (see Figure 5). This "phase-reversal-component" shows a characteristic development for each specific recording site.

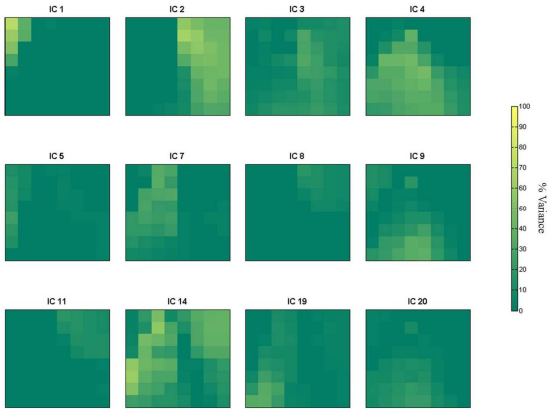

Fig. 4. Examples of independent component maps. Spatial distribution of twelve components extracted from Patient_1 dataset. Maps are obtained by plotting the percent variance accounted for the considered component of all electrode signals by keeping their relative position within the array. Electrodes in light-green have the highest PVAF, implying the prevalence of such single component. Components are on electrodes with accurate spatial definition, allowing to identify, for every component, a subset of electrodes within the array. In particular, the IC14 seems to provide the best indication about central sulcus location showing a PVAF greater than zero only for electrodes involved in phase-reversal.

Waveform differences are based on polarity and latency, with P20-N30 pattern on the motor cortex and N30-P20 pattern on the somatosensory cortex. As a consequence,

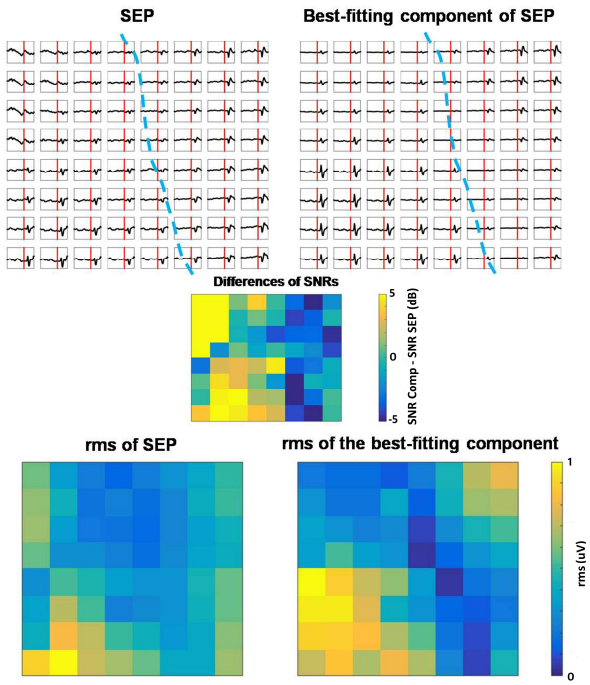

Fig. 5. Comparison between SEP and back-projection of the component that best fits the location of the central sulcus for Patient_1. Every black line corresponds to the time series (-100ms before the median nerve stimulation and 60 ms after) respectively for SEP and for the back-projection on all electrodes of the component which shows a polarity inversion between motor and somatosensory cortex. Based on this inversion of polarity the dotted blue lines show where the central sulcus path approximately lies. The root-mean-square (rms) of SEP and the selected component are shown in the two color maps at the bottom of the figure. Note that the central sulcus location is more easily identified thanks to the color contrast found in the component-rms map. The color map in the middle shows the difference between the SNR of the same signals for each electrode. The mean difference over all electrodes is positive (mean±SEM = 0.80±0.63), therefore the phase-reversal component carries more information about the signal and it is less noisy.

the reduced signal intensity of phase-reversal-component between the two cortical areas provides a clear landmark of the sulcus. A more direct identification of the sulcus location can be obtained by representing the signal through rms values (see Figure 5 for Patient_1). The color contrast in the component-rms map allows to easily detect the border between the two areas, which is less evident in the SEP-rms map. The advantage of decomposing the signal into ICs is quantified by the SNR analysis, which shows that the stimulation-related signal (i.e. the two peaks caused by the stimulation) is higher for the back-projection of phase-reversal component than for the simple SEP signal. Difference for each electrode of SNR between the two signals have been plotted through a color map and the average of differences over all electrodes have been calculated (dSNR) (see Figure 5 for Patient_1). For all patients the SNR related to the phase-reversal component is higher with a positive mean difference (mean ± SEM for each patient: P_1: dSNR=0.80±0.63; P_2: dSNR=9.46±0.62; P_3: dSNR=10.12±0.48).

In order to verify component mapping reliability at a single-trial level, we analyzed PVAF for each trial of the three recording sessions by back-projecting components on every time series epoch. Due to the large number of selected trials, we compressed all figures in a video (see multimedia Movie1) showing the dynamics of spatial structure components for all single trials of Patient_1, from the first to the last one (n=250). Despite the expected variability among trials, spatial maps of some components are highly reliable, practically involving the same electrodes throughout all trials. For example, in no trial IC1 is on the array top right corner, while IC14, the phase-reversal-component, allows to 'track' the central sulcus in most trials. The reliability at single trial level is also confirmed by the signal-to-noise ratio analysis which showed for all patients that the phase-reversal component carries more stable information than the SEP signal itself (results not shown).

3.4 Absence of correlation between ICs and electrode impedance

Since the electrode impedance variability among all electrodes might affect the topography of the component maps, the normalized magnitude impedance at 30 Hz has been plotted for all subjects by using green-scale color maps as in Figure 4. We have chosen this value because it corresponds in the frequency domain to the phase-reversal pattern characterized in the time domain by a peak around 20ms and an inversion of polarity around 30ms. Figure 6 shows the impedance maps at 30 Hz for the arrays used to record the SEP activity of all three patients. The impedance values (mean ± SEM for 64 electrodes) are respectively 540.9±8.5kΩ, 463.2±8.1kΩ and 572.9±7.1kΩ. A direct comparison of the impedance maps with the paths of the central sulcus (represented in the Figure 6 by dotted blue lines) and the spatial distributions of independent components (Figure 4), do not show any similarity. Therefore impedance variability of electrodes did not affect the components distribution.

4. Discussion

To the best of our knowledge, this is the first study in which ICA has been applied to high-density micro-ECoG data to investigate independent components subtending neural response elicited by median nerve stimulation. Several studies on scalp recordings and on intracranial EEG recordings used ICA as a tool to suppress artifacts of muscle activity and eye blinks, or to demonstrate the wide distribution of functional networks [17], [18], [19], [20], [21], [22], [37], [38], [44], [45], [46], [47], [48], [49], [50]. In this study we applied ICA to micro-ECoG data provided by custom made micro-ECoG arrays with sub-millimeter spatial resolution, demonstrating that our approach can improve the discrimination of fine segregate functional neural signals.

4.1 Decomposition of sub-millimeter ECoG data into independent components

We applied ICA to high density SEPs, because changing the domain of neural signal processing, from electrode signals to sources that generate such signals, could be instructive. This study focused on SEP data acquired epicortically through a probe with 18.49 mm^2 recording area subdivided into 64 individual electrodes. Given the close proximity of recording electrodes, volume-conduction effects cannot be neglected. Thus, signals from close electrodes might appear very similar while efforts to obtain such spatial resolution could be unjustified. Moreover, signal variability, caused by different contact impedance of individual electrodes, might be confused with meaningful physiological patterns.

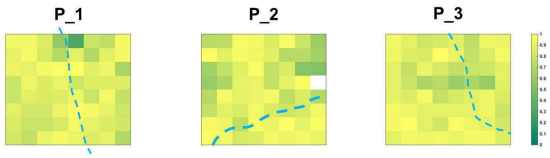

Fig. 6. Green-scale color map of normalized magnitude impedance at 30 Hz for all subjects. Such frequency value is characteristic for the phase-reversal pattern. The maps do not show any similarity with the central sulcus paths (dotted blue lines) and with the PVAF-maps of components (see Figure 4 for Patient_1).

We firstly determined whether from such dataset we could extract signals holding greater independence. We applied ICA to decompose neural signals into a set of maximally temporally independent components and tested their correlation compared to the original data. R2 histogram demonstrated that ICA decomposed original neural activity of all patients into a set of components with much greater independence among signals than the original neural signals.

The contribution of each component to the original signal was expressed through PVAF measurements which quantified the relationship between components and electrodes. Given the matrix geometry, we were able to display a 2-D map for each considered component by plotting its contribution to the signal of all electrodes. The components contribute to electrode signals in different ways, but no one electrode showed a 100% variance accounted for one single component. This means that there is no univocal association between sources and recording sites. The sources, indeed, project to multiple electrodes and the maps (see Figure 4, Figure 5) showed that every component is characterized by its own spatial distribution. Thanks to the central sulcus landmark, spatial patterns are biologically validated. For all subjects ICA extracted one phase-reversal-component that changes polarity depending on recording site (see Figure 5).

This component offered a clear identification of the central sulcus path, as shown by the rms maps, and it also provided a substantial improvement in term of SNR in understanding a neural pattern already visible by averaging the electrode signals over multiple trials.

We also tested whether the impedance variability among electrodes affected the spatial distribution of components. Impedance maps at 30Hz of the electrode arrays used for recordings did not show any similarity with the central sulcus paths (see Figure 6). This evaluation further confirmed that ICA can decompose high density ECoG data into signals characterized by biologically plausible spatial maps. Thanks to the presence of both the anatomical marker of central sulcus and the functional landmark of phase-reversal we were able to assess the reliability of our approach at the spatial resolution of our arrays.

Sub-millimeter spatial definition of component distribution encourages the development of new approaches to locate the sources responsible for abnormal activities in neurological disorders like epilepsy or infiltrating tumors. ICA technique has been already applied to investigate and identify signal components with seizure-like patterns [20], [21], [22], [50], [51]. The success of surgical procedures strongly depends on accurate site identification of the lesion borders. Our ICA for micro-ECoG data, eventually combined to a realistic brain model, may be a useful tool to identify the exact site and borders of pathological brain regions with micrometric accuracy.

4.2 Micro-sources and Brain Computer Interface

We extracted independent components at single trial level and calculated related PVAF of all electrodes. Each trail has been used as a frame of a movie (see multimedia Movie 1) to show the spatial-temporal development of PVAF maps. Despite the expected variability among trials, components showed strongly stable spatial patterns throughout stimulation. Moreover the reliability at single trial level of the phase-reversal component over the SEP signal is further confirmed by the SNR analysis (results not shown).

This result opens new perspectives for Brain Computer Interface (BCI). The key point of BCI, indeed, is the capability of the decoder to discriminate meaningful signal features at single-trial level and many studies have been focused precisely on improving the features extraction [52], [53], [54], [55], [56], [57], [58], [59]. He Bin and collaborators have clearly shown the benefits from adopting a source analysis approach to classify motor imagery tasks in humans [15], [60]. By switching from sensors to sources, they have been able to increase the mean classification accuracy in discriminating hand movements in three subjects by a factor of 9.2%. Thus, component analysis has identified

temporal-spectral-spatial biomarkers subtending the task leading to greater differentiation of stimuli, which in turn can lead to increase the efficacy of decoding algorithms for BCI applications [15].

In this work, we have demonstrated that source analysis is reliable for micro-ECoG data interpretation, which, thanks to a small recording array size and its extremely localized dense spatial sampling, is a promising tool for chronic BCIs.

5. Conclusions

To conclude, micro-ECoG recordings combined with suitable source analysis open up new and powerful perspectives for deeper understanding of brain and cognitive functions. We demonstrated that ICA decomposition can isolate, out of high density data, different components with biologically plausible spatial distribution and that are reliable at single trial level. This important result highlighted the advantages of employing microelectrode probes in ECoG recordings, providing evidence of the feasibility to resolve independent signals at sub-millimeter scale. Several benefits arise from micro-ECoG array adoption, ranging from high reliability to the reduced invasiveness. Moreover, as we have shown, micro-ICA provides a reliable fine segregation of functional units. It could be applied to identify the sites of pathological sources for clinical purposes, or it could improve the decoding performance for discriminating neural patterns subtending motor or cognitive tasks for BCI applications.

Acknowledgements

The authors declare no competing financial interests.

The authors would like to thank the team of the Neurosurgery Department of the Azienda Ospedaliero-Universitaria S.M.M. of Udine for the precious assistance and help provided throughout the entire data collection process (in particular Quinto Sbrizzai for his technical support). This work was supported by the BMI project of the Italian Institute of Technology and by MIUR (PRIN 2012) Grant to LF.

References

1. Leuthardt EC, Schalk G, Wolpaw JR, Ojemann JG, Moran DW.A brain-computer interface using electrocorticographic signals in humans. Neural eng. 2004 ; 1, 63-71.
2. Schalk G, Miller KJ, Anderson NR, Wilson JA, Smyth MD, Ojemann JG, Moran DW, Wolpaw JR, Leuthardt EC. Two-dimensional movements control using electrocorticographic signals in humans. J Neural Eng. 2008 Mar; 5(1): 75:84.
3. Miller KJ, Zanos S, Fetz EE, Den Nijs M, Ojemann JG. Decoupling the cortical power spectrum reveals real-time representation of individual finger movements in humans. J Neurosci. 2009 Mar 11; 29(10): 3132-7
4. Pistohl T, Ball T, Schulze-Bonhage A, Aertsen A, Mehring C. Prediction of arm movement trajectories from ECoG-recordings in humans. J Neurosci Methods. 2008 Jan; 167(1): 105-14.
5. Yanagisawa T, Hirata M, Saitoh Y, Goto T, Kishima H, Fukuma R, Yokoi H, Kamitani Y, Yoshimine T. Real-time control of a prosthetic hand using human electrocorticography signals. J Neurosurg. 2011 Jun; 114(6): 1715-22.
6. Chao ZC, Nagasaka Y, Fujii N. Long-term asynchronous deconding of arm motion using electrocorticographic signals in monkeys. Front Neuroeng. 2010 Mar; 3:3.
7. Ball T, Kern M, Mutschler L, Aertsen A, Schulze-Bonhage A. Signal quality of simultaneously recorded invasive and non-invasive EEG. Neuroimage 2009 Jul; 46(3): 708-16.
8. Castagnola E., Ansaldo A., Maggiolini E., Angotzi G.N., Skrap M., Ricci D., Fadiga L. Biologically compatible neural interface to safely couple nanocoated electrodes to the surface of the brain. ACS Nano. 2013 May; 7(5): 3887-95.
9. Viventi J, Kim DH, Vigeland L, Frechette ES, Blanco JA, Kim YS, Avrin AE, Tiruvadi VR, Hwang SW, Vanleer AC, Wulsin DF, Davis K,Gelber CE, Palmer L, Van der Spiegel J, Wu J, Xiao J, Huang Y, Contreras D, Rogers JA, Litt B. Flexible, foldable, actively multiplexed, high-density electrode array for mapping brain activity in vivo. Nat Neurosci. 2011 Nov 13;14(12):1599-605.
10. Viventi J, Blanco JA. Development of high resolution, multiplexed electrode arrays: Opportunities and challenges. Conf Proc IEEE Eng Med Biol Soc. 2012 Aug;2012:1394-6.
11. Zeki SM. Functional specialization in the visual cortex of the rhesus monkey. Nature. 1978 Aug 3;274(5670):423-8.
12. Morel A, Garraghty PE, Kaas JH. Tonotopic organization, architectonic fields, and connections of auditory cortex in macaque monkeys. J Comp Neurol. 1993 Sep 15;335(3):437-59.
13. Nunez PL, Wingeier BM, Silberstein RB. Spatial-temporal structures of human alpha rhythms: theory, microcurrent sources, multiscale measurements, and global binding of local networks. Hum Brain Mapp. 2001 Jul;13(3):125-64.

14. Nunez PL, and Srinivasan R. Electric Fields of the Brain : The neurophysics of EEG. 2006 Oxford University Press.
15. Edelman B., Baxter B., He B. Decoding and mapping of right hand motor imagery tasks using EEG sources imaging. 2015. 7th annual international IEEE EMBS conference of neural engineering.
16. Bell AJ, and Sejnowski TJ. An information-maximization approach to blind separation and blind deconvolution. Neural Comput. 1995 Nov;7(6):1129-59.
17. Makeig S, Jung TP, Bell AJ, Ghahremani D, Sejnowski TJ. Blind separation of auditory event-related brain responses into independent components. Proc Natl Acad Sci U S A. 1997 Sep 30;94(20):10979-84.
18. Jung TP, Makeig S, Humphries C, Lee TW, McKeown MJ, Iragui V, Sejnowski TJ. Removing electroencephalographic artifacts by blind source separation. Psychophysiology. 2000 Mar;37(2):163-78.
19. Delorme A, Sejnowski T, Makeig S. Enhanced detection of artifacts in EEG data using higher-order statistics and independent component analysis. Neuroimage. 2007 Feb 15;34(4):1443-9.
20. Acar ZA, Makeig S, Worrell G. Head modeling and cortical source localization in epilepsy. Conf Proc IEEE Eng Med Biol Soc. 2008: 3763-6.
21. Acar ZA, Worrell G, Makeig S. Patch-basis electrocortical source imaging in epilepsy. Conf Proc IEEE Eng Med Biol Soc. 2009: 2930-3.
22. Mullen T, Worrell G, Makeig S. Multivariate principal oscillation pattern analysis of ICA sources during seizure. Conf Proc IEEE Eng Med Biol Soc. 2012 Aug;2012:2921-4.
23. Dewar S, Passaro E, Fried I, Engel J Jr. Intracranial electrode monitoring for seizure localization: indications, methods and the prevention of complications. J Neurosci Nurs. 1996 Oct;28(5):280-4, 289-92.
24. Baghdadi TS, and Najjar MW. Evaluation of intractable epilepsy. Invasive monitoring. Neurosciences (Riyadh). 2010 Apr;15(2):71-8.
25. Berger MS, Kincaid J, Ojemann GA, Lettich E. Brain mapping techniques to maximize resection, safety, and seizure control in children with brain tumors. Neurosurgery. 1989 Nov; 25(5): 786-92.
26. Berger MS, and Ojemann GA. Intraoperative brain mapping techniques in neuro-oncology. Stereotact Funct Neurosurg 1992; 58, 153-61.
27. Duffau, H., Capelle, L., Denvil, D., Gatignol, P., Sichez, N., Lopes, M., Sichez, J. P. & Van Effenterre, R. The role of dominant premotor cortex in language: a study using intraoperative functional mapping in awake patients. Neuroimage 2003; 20, 1903-14.
28. Skrap M., Mondani M., Tomasino B., Weis L., Budai R., Pauletto G., Eleopra R., Fadiga L. & Ius T. Surgery of insular non-enhancing Gliomas: volumetric analysis of tumoral resection, clinical outcome and survival in a consecutive series of 66 cases. Neurosurgery. 2011.
29. Allison T, McCarthy G, Wood CC, Jones SJ. Potentials evoked in human and monkey cerebral cortex by stimulation of the median nerve. A review of scalp and intracranial recordings. Brain. 1991 Dec;114 (Pt 6):2465-503.
30. Baumgärtner U, Vogel H, Ohara S, Treede RD, Lenz FA. Dipole source analyses of early median nerve SEP components obtained from subdural grid recordings. J Neurophysiol. 2010 Dec;104(6):3029-41.
31. Lüders H, Lesser RP, Hahn J, Dinner DS, Klem G. Cortical somatosensory evoked potentials in response to hand stimulation. J Neurosurg. 1983; 58, 885-894.
32. Gregorie EM and Goldring S, Localization of function in the excision of lesions from the sensorimotor region. J Neurosurg. 1984; 61, 1047-1054.
33. Allison T, McCarthy G, Wood CC, Darcey TM, Spencer DD, Williamson PD. Human cortical potentials evoked by stimulation of the median nerve. I. Cytoarchitectonic areas generating short-latency activity. J Neurophysiol. 1989 Sep;62(3):694-710.
34. Fukuda M, Nishida M, Juhász C, Muzik O, Sood S, Chugani HT, Asano E. Short-latency median-nerve somatosensory-evoked potentials and induced gamma-oscillations in humans. Brain. 2008 Jul;131(Pt 7):1793-805. Epub 2008 May 27.
35. Castagnola E., Ansaldo A. Maggiolini E., Ius T., Skrap M., Ricci D. Fadiga L. Smaller, softer, lower-impedence electrodes for human neuroprosthesis: a pragmatic approach. Front Neuroeng 2014 Apr; 7:8.
36. American Clinical Neurophysiology Society. Guideline 9A: Guidelines on Evoked Potentials. Journal of Clinical Neurophysiology. 23(2):125-137, April 2006.
37. Delorme A, Makeig S. EEGLAB: an open source toolbox for analysis of single-trial EEG dynamics including independent component analysis. J Neurosci Methods. 2004 Mar 15;134(1):9-21.
38. Jung TP, Makeig S, Bell AJ, Sejnowski TJ. Independent component analysis of electroencephalographic and event-related potential data. Central Auditory Processing and Neural Modelin,, New York, 1998.
39. Burnos S, Fedele T, Schmid O, Krayenbühl N, Sarnthein J. Detectability of the somatosensory evoked high frequency oscillation (HFO) co-recorded by scalp EEG and ECoG under propofol. Neuroimage: Clinical 2016; 10,318-325.
40. Makeig S, Onton J. ERP features and EEG dynamics: an ICA perspective. Oxford Handbook of event-related potential components. New York, Oxford University Press 2011.
41. Charkhkar H, Knaack GL, McHail DG, Mandal HS, Peixoto N, Rubinson JF, Dumas TC, Pancrazio JJ. Chronic intracortical neural recordings using microelectrode arrays coated with PEDOT–TFB. Acta Biomaterialia 2016; 32, 57-67.
42. Ludwig KA, Uram JD, Yang J, Martin DC, Kipke DR, Chronic neural recordings using silicon microelectrode arrays electrochemically deposited with a poly(3,4-

ethylenedioxythiophene) (PEDOT) film, J. Neural Eng. 2006; 3, 59.

43. Suner S, Fellows MR, Vargas-Irwin C, Nakata GK, Donoghue JP, Reliability of signals from a chronically implanted, silicon-based electrode array in nonhuman primate primary motor cortex, IEEE Trans. Neural Syst. Rehabil. Eng. 2005; 13, 524–541.
44. Anemüller J, Sejnowski TJ, Makeig S. Complex independent component analysis of frequency-domain electroencephalographic data. Neural Netw. 2003 Nov;16(9):1311-23.
45. Hu S, Stead M, Worrell GA. Automatic identification and removal of scalp reference signal for intracranial EEGs based on independent component analysis. IEEE Trans Biomed Eng. 2007 Sep;54(9):1560-72.
46. Whitmer D, Worrell G, Stead M, Lee IK, Makeig S. Utility of independent component analysis for interpretation of intracranial EEG. Front Hum Neurosci. 2010 Nov 2;4:184.
47. Chan HL, Chen YS, Chen LF. Selection of independent components based on cortical mapping of electromagnetic activity. J Neural Eng. 2012 Oct;9(5).
48. Santillan-Guzman A, Heute U, Stephani U, Galka A. Muscle artifact suppression using Independent-Component Analysis and State-Space Modeling. Conf Proc IEEE Eng Med Biol Soc. 2012 Aug; 6500-3.
49. Szibbo D, Luo A, Sullivan TJ. Removal of blink artifacts in single channel EEG. Conf Proc IEEE Eng Med Biol Soc. 2012 Aug; 3511-4.
50. Yoshida H, Tanaka Y, Kikkawa S. EEG analysis of frontal lobe area in arousal maintenance state against sleepiness. Conf Proc IEEE Eng Med Biol Soc. 2012 Aug; 2933-6.
51. Ghosh-Dastidar S, Adeli H, Dadmehr N. Principal Component Analysis-Enhanced Cosine Radial Basis Function Neural Network for Robust Epilepsy and Seizure Detection. IEEE Transactions on Biomedical Engineering. 2008; 55:2, 512-518.
52. Nakanishi M, Wang Y, Wang YT, Mitsukura Y, Jung TP. A High-speed Brain Speller Using Steady-state Visual Evoked Potentials. International Journal of Neural Systems 2014; 24:6, 1450019.
53. Zhang Y, Zhou G, Jin J, Zhao Q, Wang X, Cichocki A. Aggregation of Sparse Linear Discriminant Analyses for Event-related Potential Classification in Brain-Computer Interface. International Journal of Neural Systems 2014; 24:1, 1450003.
54. Li J, Ji H, Cao L, Zang D, Gu R, Xia B. Evaluation and application of a hybrid brain computer interface for real wheelchair control with multi-degrees of freedom. International Journal of Neural Systems 2014; 24:4, 1450014.
55. Ortiz-Rosario A, Adeli H. Brain-Computer Interface Technologies: From signal to action. Reviews in the Neurosciences 2013; 24:5, 537-552.
56. Ortiz-Rosario A, Adeli H, Buford JA. Wavelet Methodology to Improve Single Unit Isolation in Primary Motor Cortex Cells. Journal of Neuroscience Methods 2015; 246, 106-118.
57. Jin J, Sellers EW, Zhou S, Zhang Y, Wang X, Cichocki A. A P300 brain computer interface based on a modification of the mismatch negativity paradigm. International Journal of Neural Systems 2015; 25:3, 1550011.
58. Zhang D, Huang B, Li S, Wu W. An idle-state detection algorithm for SSVEP-based brain-computer interfaces using a maximum evoked response spatial filter. International Journal of Neural Systems 2015; 25:7, 1550030.
59. Jin J, Allison BZ, Zhang Y, Wang X, Cichocki A. An ERP-based BCI using an oddball paradigm with different faces and reduced errors in critical functions. International Journal of Neural Systems 2014; 24:8, 1450027.
60. Qin L., Ding L., He B. Motor Imagery classification by means of source analysis for brain computer interface applications. J Neural Eng. 2005 Dec; 2(4): 65-72.